

PREDICTION OF THE DEFORMATION BEHAVIOR OF SAND SUBJECTED TO GENERAL CYCLIC LOADING BY THE TANGENTIAL-SUBLOADING SURFACE MODEL

H. Setouchi¹, K. Hashiguchi² and M. Ueno³

ABSTRACT: The traditional elastoplastic constitutive equations can not generally describe the inelastic deformation considering the magnitude and the direction of the stress rate. Therefore, the stiffness is unrealistically predicted in the nonproportional loading. The *tangential-subloading surface model* by Hashiguchi and Tsutsumi (2001) can describe the dependence of both the magnitude and the direction of the inelastic strain rate on the stress rate. In this paper, the *tangential strain rate* induced by the stress rate component tangential to the yield surface is incorporated into the *extended subloading surface model* to describe the cyclic loading behavior. The model is applied to the prediction of the deformation behavior of sand subjected to general cyclic loading including the proportional and nonproportional loadings. The validity of the model is verified by comparing with experimental results.

Keywords: Cyclic loading, elastoplasticity, inelastic strain rate, nonproportional loading, subloading surface model, tangential stress rate

INTRODUCTION

The breakwater is the important structure in order to keep functions and safety of various facilities in the lowland. However, the soft ground in the lowland can not bear the weight of the breakwater. Hence the soft soils in the lowland are frequently replaced by sand to prepare foundation ground. The sand foundation is required to have strength for not only the dead weight of the breakwater but also the cyclic loading by the wave and seismic forces. Further, the nonproportional loading occurs in combining these forces. It is also important to describe the elastoplastic behavior in order to predict the deformation problem, which such force causes.

A rigorous formulation of the unconventional elastoplastic constitutive equation (Drucker, 1988) enabling the description of plastic strain rate due to the stress rate inside the yield surface have been attained by the *subloading surface model* (Hashiguchi and Ueno, 1977; Hashiguchi, 1980). The subloading surface which always passes through the current stress point and is similar to the yield surface, renamed the *normal-yield surface*, is assumed inside the normal-yield surface. The model can describe the anisotropy of the material and the plastic deformation is described by adopting the *associated flow rule*. The subloading surface model has also been extended

to describe the cyclic loading behavior (Hashiguchi, 1989) by letting the similarity-center of the normal-yield and the subloading surfaces translate with the plastic deformation, which is called the *extended subloading surface model*. The model fulfills the mechanical requirements for constitutive equations (Hashiguchi, 1993a, 1993b), i.e. the continuity condition, the smoothness condition, the work rate-stiffness relaxation and the Masing effect. It has been applied to the prediction of deformation behavior of soils (Topolnicki, 1990; Hashiguchi and Chen, 1998) and metals (Hashiguchi and Yoshimaru, 1995).

However, in the traditional elastoplastic constitutive equations, unrealistically stiff response is predicted for the analysis of the plastic instability phenomena in which the stress path deviates from the proportional loading since the plastic strain rate is independent of the magnitude and the direction of the stress rate. Therefore, the subloading surface model has been further extended so as to describe the strain rate, called the *tangential strain rate*, induced by the stress rate component tangential to the subloading surface, called the *tangential stress rate* (Hashiguchi and Tsutsumi, 2001). Such a model is called the *tangential-subloading surface model*. The model can describe the dependence of both the magnitude and the direction of the inelastic strain rate on the stress rate. The subloading surface model with the tangential strain rate, i.e. the

¹ Research Associate, University of the Ryukyus, 903-0213, JAPAN

² Professor, Kyushu University, 812-8581, JAPAN

³ Professor, University of the Ryukyus, 903-0213, JAPAN

Note: Discussion on this paper is open until December 2005

tangential-subloading surface model, has been applied to the prediction of the bifurcation phenomena in deformation of soils (Hashiguchi and Tsutsumi, 2001, 2003; Khojastehpour and Hashiguchi, 2004a, 2004b) and metals (Hashiguchi and Protasov, 2004) predicting the formation of shear bands and/or diffuse modes of deformation as the bulging and buckling.

In this article, the tangential strain rate is incorporated into the extended subloading surface model to describe the cyclic loading behavior. The extended subloading surface model with the tangential strain rate is then applied to the prediction of the deformation behavior in sand subjected to cyclic loading under not only the proportional loading but also the nonproportional loading. The validity of the model is verified by comparing with the experimental results.

The signs of stress (rate) and strain rate (a symmetric part of velocity gradient) components are taken to be positive for tension.

OUTLINE OF THE TANGENTIAL-SUBLOADING SURFACE MODEL

In this section the extended subloading surface model with the tangential stress rate effect (Hashiguchi and Tsutsumi, 2001) is reviewed briefly. This model will be later applied to the analysis of the deformation behavior in soils subjected to the cyclic loading under the nonproportional loading.

Denoting the current configuration of material particle as \mathbf{x} and the current velocity as \mathbf{v} , the velocity gradient is described by $\mathbf{L} \equiv \partial \mathbf{v} / \partial \mathbf{x}$, by which the strain rate and the continuum spin are defined as $\mathbf{D} (\equiv (\mathbf{L} + \mathbf{L}^T) / 2)$ and $\mathbf{W} (\equiv (\mathbf{L} - \mathbf{L}^T) / 2)$, respectively, $()^T$ standing for the transpose.

Now let it be assumed that the strain rate \mathbf{D} is additively decomposed into the elastic strain rate \mathbf{D}^e and the inelastic strain rate \mathbf{D}^i which is further decomposed into the plastic strain rate \mathbf{D}^p and the *tangential strain rate* \mathbf{D}^t , i. e.

$$\mathbf{D} = \mathbf{D}^e + \mathbf{D}^i, \quad (1)$$

$$\mathbf{D}^i = \mathbf{D}^p + \mathbf{D}^t, \quad (2)$$

where the elastic strain rate \mathbf{D}^e is given by

$$\mathbf{D}^e = \mathbf{E}^{-1} \overset{\circ}{\boldsymbol{\sigma}}. \quad (3)$$

$\boldsymbol{\sigma}$ is the *Cauchy stress* and $\overset{\circ}{(\)}$ indicates the proper corotational rate with the objectivity (e.g. Dafalias, 1985; Zbib and Aifantis, 1988) and the fourth-order tensor \mathbf{E} is the elastic modulus given in the Hooke's type as

$$E_{ijkl} = (K - \frac{2}{3}G)\delta_{ij}\delta_{kl} + G(\delta_{ik}\delta_{jl} + \delta_{il}\delta_{jk}), \quad (4)$$

where K and G are the bulk and shear modulus, respectively, which are functions of stress and internal state variables in general and δ_{ij} is the Kronecker's delta, i.e. $\delta_{ij} = 1$ for $i = j$ and $\delta_{ij} = 0$ for $i \neq j$.

Normal-yield and Subloading Surfaces

Assume the yield condition:

$$f(\hat{\boldsymbol{\sigma}}, \mathbf{H}) = F(H), \quad (5)$$

where

$$\hat{\boldsymbol{\sigma}} \equiv \boldsymbol{\sigma} - \boldsymbol{\alpha}. \quad (6)$$

The second-order tensor $\boldsymbol{\alpha}$ is the reference point inside the yield surface, which plays the role of the kinematic hardening variable as it translates with the plastic deformation. The second-order tensor \mathbf{H} and the scalar H are the inherent or induced anisotropic hardening and isotropic hardening/softening variables, respectively. Let it be assumed that the function f is homogeneous of degree one in the tensor $\hat{\boldsymbol{\sigma}}$, satisfying $f(s\hat{\boldsymbol{\sigma}}, \mathbf{H}) = sf(\hat{\boldsymbol{\sigma}}, \mathbf{H})$ for any nonnegative scalar s . Then, if $\mathbf{H} = \text{constant}$, the yield surface keeps the similar shape and translates with $\boldsymbol{\alpha}$. The inherent and the induced anisotropy of soils can be described concisely by the *rotational hardening*, whilst the kinematic hardening is inapplicable to soils as has been described by Hashiguchi (2001).

Hereinafter, let the elastoplastic constitutive equation be formulated in the framework of the *unconventional plasticity* defined by Drucker (1988). The interior of yield surface is not a purely elastic domain but plastic deformation is induced by the rate of stress inside the yield surface. Thus, the conventional yield surface is renamed as the *normal-yield surface*, since its interior is not regarded as a purely elastic domain in the present model.

Now, let the *subloading surface* (Hashiguchi and Ueno, 1977; Hashiguchi, 1980, 1989) be introduced, which always passes through the current stress $\boldsymbol{\sigma}$ and keeps the similarity and the configuration of similarity to the normal-yield surface. All lines passing through arbitrary conjugate pair of points on these surfaces joint at the specified point, i.e. the *similarity-center* which will be denoted by \mathbf{s} . In addition, let it be assumed that the subloading surface, which plays the role of loading surface, does not intersect the normal-yield surface. Therefore, the similarity-center has to be inside the normal-yield surface. The ratio of the size of the subloading surface to that of the normal-yield surface will be denoted by R ($0 \leq R \leq 1$) which can be regarded as the measure of approaching degree to the normal-yield state and is thus called the *normal-yield ratio*.

The conjugate stress σ_y on the normal-yield surface for the current stress σ on the subloading surface due to the similarity is given by

$$\sigma_y = \frac{1}{R} \{ \sigma - (1-R)s \}, \quad (\sigma - s = R(\sigma_y - s)) \quad (7)$$

By substituting Eq. (7) into Eq. (5) with regard to $\hat{\sigma}$ as σ_y , the subloading surface is described as

$$f(\bar{\sigma}, \mathbf{H}) = RF(H), \quad (8)$$

where

$$\begin{aligned} \bar{\sigma} &\equiv \sigma - \bar{\alpha}, & (9) \\ \bar{\alpha} &\equiv s - R(s - \alpha). & (10) \end{aligned}$$

Here $\bar{\alpha}$ inside the subloading surface is the conjugate point of α inside the normal-yield surface. The normal-yield and the subloading surfaces are illustrated in Fig. 1.

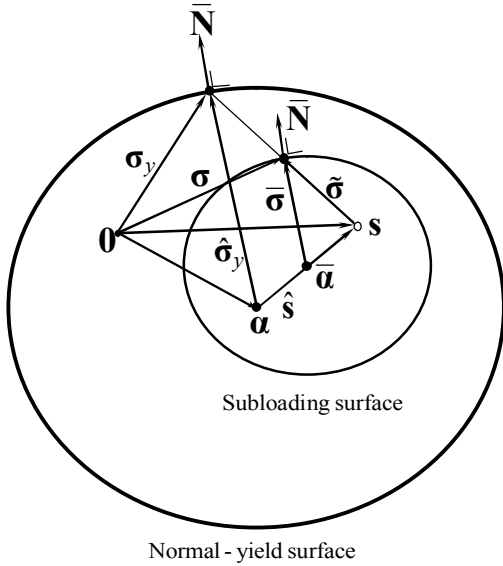


Fig. 1 Normal-yield and subloading surfaces

Evolution Rule of Normal-yield Ratio

Taking account of the fact that a stress asymptotically approaches the normal-yield surface, i.e. the subloading surface approaches the normal-yield surface in the plastic loading process, let the evolution rule of the normal-yield ratio R be given by

$$\dot{R} = U \|\mathbf{D}^p\| \text{ for } \mathbf{D}^p \neq \mathbf{0}, \quad (11)$$

where U is the monotonically decreasing function of R , satisfying

$$\left. \begin{aligned} U &= +\infty \text{ for } R = 0, \\ U &= 0 \text{ for } R = 1, \\ (U < 0 \text{ for } R > 1). \end{aligned} \right\} \quad (12)$$

(*) stands for the material-time derivative, $\|\cdot\|$ stands for the magnitude, i.e. $\|\mathbf{T}\| = \sqrt{\text{tr}(\mathbf{T}\mathbf{T}^T)}$, $\text{tr}(\cdot)$ denoting the trace. Let the function U satisfying Eq. (12) be simply given by

$$U = -u_R \ln R, \quad (13)$$

where u_R is a material constant.

Translation Rule of Similarity-center

The similarity-center s is required to translate with the plastic deformation in order to describe realistically the cyclic loading behavior exhibiting the Masing effect (Masing, 1926; Mroz, 1966; Hashiguchi, 1993b). The translation rule of the similarity-center s is given as

$$\dot{s} = c_s \|\mathbf{D}^p\| \left\{ \frac{\tilde{\sigma}}{R} + \dot{\alpha} + \frac{1}{F} \left[\dot{F} - \text{tr} \left(\frac{\partial f(\hat{s}, \mathbf{H})}{\partial \mathbf{H}} \dot{\mathbf{H}} \right) \right] \right\} \hat{s}, \quad (14)$$

where

$$\begin{aligned} \tilde{\sigma} &\equiv \sigma - s, & (15) \\ \hat{s} &\equiv s - \alpha. & (16) \end{aligned}$$

c_s is a material constant.

Plastic Strain Rate

The time-differentiation of Eq. (8) has the *extended consistency condition* for the subloading surface:

$$\begin{aligned} \text{tr} \left(\frac{\partial f(\bar{\sigma}, \mathbf{H})}{\partial \bar{\sigma}} \dot{\bar{\sigma}} \right) - \text{tr} \left(\frac{\partial f(\bar{\sigma}, \mathbf{H})}{\partial \bar{\sigma}} \dot{\bar{\alpha}} \right) + \text{tr} \left(\frac{\partial f(\bar{\sigma}, \mathbf{H})}{\partial \mathbf{H}} \dot{\mathbf{H}} \right) \\ = U \|\mathbf{D}^p\| \left[F + RF' \dot{H} \right], \end{aligned} \quad (17)$$

where

$$F' \equiv \frac{dF}{dH}. \quad (18)$$

Assume the associated flow rule for the subloading surface

$$\begin{aligned} \mathbf{D}^p &= \lambda \bar{\mathbf{N}}, & (19) \\ \bar{\mathbf{N}} &\equiv \frac{\partial f(\bar{\sigma}, \mathbf{H})}{\partial \bar{\sigma}} / \left\| \frac{\partial f(\bar{\sigma}, \mathbf{H})}{\partial \bar{\sigma}} \right\| \quad (\|\bar{\mathbf{N}}\| = 1), & (20) \end{aligned}$$

where λ is the positive proportionality factor. The second-order tensor $\bar{\mathbf{N}}$ is the normalized outward-normal of the subloading surface.

The substitution of Eq. (19) into the extended consistency condition Eq. (17) leads to

$$\lambda = \frac{\text{tr}(\bar{\mathbf{N}} \dot{\hat{\boldsymbol{\sigma}}})}{\bar{M}_p}, \quad (21)$$

where

$$\bar{M}_p \equiv \text{tr} \left[\bar{\mathbf{N}} \left(\left\{ \frac{F'}{F} h - \frac{1}{RF} \text{tr} \left(\frac{\partial f(\bar{\boldsymbol{\sigma}}, \mathbf{H})}{\partial \mathbf{H}} \mathbf{h} \right) + \frac{U}{R} \right\} \bar{\boldsymbol{\sigma}} + \bar{\mathbf{a}} \right) \right]. \quad (22)$$

h , \mathbf{h} and $\bar{\mathbf{a}}$ are the functions of the stress, plastic internal state variables and $\bar{\mathbf{N}}$ in degree one. These functions are related to \dot{H} , $\dot{\mathbf{H}}$ and $\dot{\mathbf{a}}$ by

$$h \equiv \frac{\dot{H}}{\lambda}, \quad \mathbf{h} \equiv \frac{\dot{\mathbf{H}}}{\lambda}, \quad (23)$$

$$\bar{\mathbf{a}} \equiv \frac{\dot{\mathbf{a}}}{\lambda} = \mathbf{z} - U(\mathbf{s} - \mathbf{a}) - R(\mathbf{z} - \mathbf{a}), \quad (24)$$

$$\mathbf{a} \equiv \frac{\dot{\mathbf{a}}}{\lambda}, \quad (25)$$

$$\mathbf{z} \equiv \frac{\dot{\mathbf{s}}}{\lambda} = c_s \frac{\dot{\hat{\boldsymbol{\sigma}}}}{R} + \mathbf{a} + \frac{1}{F} \left\{ F' h - \text{tr} \left(\frac{\partial f(\hat{\mathbf{s}}, \mathbf{H})}{\partial \mathbf{H}} \mathbf{h} \right) \right\} \hat{\mathbf{s}} \quad (26)$$

since \dot{H} , $\dot{\mathbf{H}}$ and $\dot{\mathbf{a}}$ include λ in degree one.

Tangential Strain Rate

The tangential strain rate is induced by the stress rate component tangential to the subloading surface, called the *tangential stress rate*, obeying the Rudnicki and Rice's (1975) conclusion that "no vertex can result from hydrostatic stress increments" based on the consideration of the sliding mechanism in the fissure model.

The tangential strain rate \mathbf{D}^t is formulated as

$$\mathbf{D}^t = \frac{1}{T} \dot{\hat{\boldsymbol{\sigma}}}_t^*, \quad (27)$$

where T is a monotonically decreasing function of R satisfying the following condition.

$$\left. \begin{aligned} T &= +\infty \text{ for } R = 0, \\ T &= \xi \text{ for } R = 1. \end{aligned} \right\} \quad (28)$$

ξ being a material function of the stress and the plastic internal variables in general. The function T , called the *tangential inelastic modulus*, satisfying Eq. (28) is simply

given by

$$T = \frac{\xi}{R^b}, \quad (29)$$

where $b(\geq 1)$ is a material constant. The second-order tensor $\dot{\hat{\boldsymbol{\sigma}}}_t^*$ is given as follows:

$$\dot{\hat{\boldsymbol{\sigma}}}_t^* \equiv \dot{\hat{\boldsymbol{\sigma}}}^* - \dot{\hat{\boldsymbol{\sigma}}}_n^*, \quad (30)$$

$$\dot{\hat{\boldsymbol{\sigma}}}_n^* \equiv \text{tr}(\bar{\mathbf{n}}^* \dot{\hat{\boldsymbol{\sigma}}}^*) \bar{\mathbf{n}}^*, \quad (31)$$

$$\dot{\hat{\boldsymbol{\sigma}}}^* \equiv \dot{\hat{\boldsymbol{\sigma}}} - \dot{\sigma}_m \mathbf{I}, \quad \sigma_m \equiv \frac{1}{3} \text{tr} \boldsymbol{\sigma}, \quad (32)$$

$$\bar{\mathbf{n}}^* \equiv \left(\frac{\partial f(\bar{\boldsymbol{\sigma}}, \mathbf{H})}{\partial \boldsymbol{\sigma}} \right)^* / \left\| \left(\frac{\partial f(\bar{\boldsymbol{\sigma}}, \mathbf{H})}{\partial \boldsymbol{\sigma}} \right)^* \right\| = \frac{\bar{\mathbf{N}}^*}{\|\bar{\mathbf{N}}^*\|} \quad (\|\bar{\mathbf{n}}^*\| = 1), \quad (33)$$

$$\bar{\mathbf{N}}^* \equiv \left(\frac{\partial f(\bar{\boldsymbol{\sigma}}, \mathbf{H})}{\partial \boldsymbol{\sigma}} \right)^* / \left\| \left(\frac{\partial f(\bar{\boldsymbol{\sigma}}, \mathbf{H})}{\partial \boldsymbol{\sigma}} \right)^* \right\| \quad (\|\bar{\mathbf{N}}^*\| \neq 1). \quad (34)$$

(\cdot) * stands for the deviatoric part, \mathbf{I} and $\bar{\mathbf{n}}^*$ are the identity tensor and the normalized deviatoric outward-normal tensor of the subloading surface, respectively. The stress rate $\dot{\hat{\boldsymbol{\sigma}}}_t^*$ is called the *deviatoric tangential stress rate* and fulfills the following equations.

$$\text{tr}(\bar{\mathbf{N}} \dot{\hat{\boldsymbol{\sigma}}}_t^*) = 0, \quad \text{tr} \dot{\hat{\boldsymbol{\sigma}}}_t^* = 0. \quad (35)$$

The deviatoric tangential stress rate $\dot{\hat{\boldsymbol{\sigma}}}_t^*$ is directed toward the tangential line of the closed curve formed by the intersection of the subloading surface and the deviatoric stress plane as illustrated in Fig. 2.

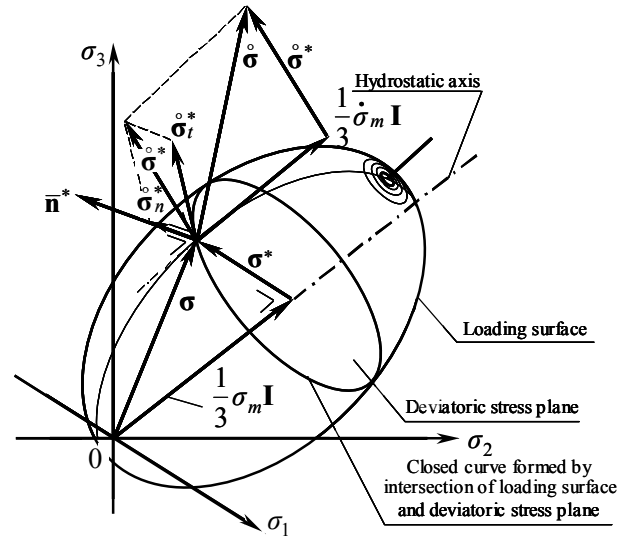


Fig. 2 The tangential stress rate $\dot{\hat{\boldsymbol{\sigma}}}_t^*$ illustrated in the principal stress space.

The strain rate \mathbf{D} is given from Eqs. (1), (2), (3), (19) and (27) as

$$\mathbf{D} = \mathbf{E}^{-1} \dot{\boldsymbol{\sigma}} + \frac{\text{tr}(\bar{\mathbf{N}} \dot{\boldsymbol{\sigma}})}{\bar{M}_p} \bar{\mathbf{N}} + \frac{1}{T} \dot{\boldsymbol{\sigma}}^* \quad (36)$$

The inverse expression of Eq. (36) is given as

$$\begin{aligned} \dot{\boldsymbol{\sigma}} = & \frac{1}{1 + \frac{2G}{T}} \left\{ \mathbf{ED} - \frac{\text{tr}(\bar{\mathbf{N}} \mathbf{ED})}{\bar{M}_p + \text{tr}(\bar{\mathbf{N}} \mathbf{EN})} \left[\mathbf{EN} + \right. \right. \\ & \left. \left. \frac{2G}{T} \left\{ \frac{1}{3} \text{tr}(\mathbf{EN}) \mathbf{I} - \left(\bar{M}_p + \frac{1}{3} \text{tr} \bar{\mathbf{N}} \text{tr}(\mathbf{EN}) \right) \frac{\bar{\mathbf{n}}^*}{\|\bar{\mathbf{N}}^*\|} \right\} \right] \right\} \\ & + \frac{2G}{T} \text{tr}(\mathbf{ED}) \left(\frac{1}{3} \mathbf{I} - \frac{1}{3} \text{tr} \bar{\mathbf{N}} \frac{\bar{\mathbf{n}}^*}{\|\bar{\mathbf{N}}^*\|} \right) \left. \right\}. \quad (37) \end{aligned}$$

The positive proportionality factor in the associated flow rule (19) is expressed in terms of the strain rate \mathbf{D} , rewriting λ as Λ , as follows:

$$\Lambda = \frac{\text{tr}(\bar{\mathbf{N}} \mathbf{ED})}{\bar{M}_p + \text{tr}(\bar{\mathbf{N}} \mathbf{EN})}. \quad (38)$$

Loading Criterion

The loading criterion is given by the positiveness of the proportionality factor Λ as follows (Hashiguchi, 2000):

$$\left. \begin{aligned} \mathbf{D}^p \neq \mathbf{0} : \Lambda > 0, \\ \mathbf{D}^p = \mathbf{0} : \Lambda \leq 0. \end{aligned} \right\} \quad (39)$$

CONSTITUTIVE EQUATION OF SOILS

Material Functions

Based on the equations formulated in previous section and the model proposed by Hashiguchi and Chen (1998), the particular forms of the material functions for soils will be given in this section. Hereafter, we focus our attention on the behavior of the saturated soils, and then let the *Cauchy stress* $\boldsymbol{\sigma}$ be meant the *effective Cauchy stress*, excluding a pore pressure u from the *total Cauchy stress* \mathbf{T} , which is defined by

$$\boldsymbol{\sigma} = \mathbf{T} + u\mathbf{I}, \quad (40)$$

where u is taken to be positive for compression.

Let the stress function of the subloading surface of Eq.

(8) be given for soils as

$$f(\bar{\boldsymbol{\sigma}}, \boldsymbol{\beta}) = \bar{p}(1 + \bar{\chi}^2), \quad (41)$$

where

$$\bar{\boldsymbol{\sigma}}^* \equiv \bar{\boldsymbol{\sigma}} + \bar{p}\mathbf{I}, \quad \bar{p} \equiv -\frac{1}{3} \text{tr} \bar{\boldsymbol{\sigma}}, \quad \bar{\chi} \equiv \frac{\|\bar{\boldsymbol{\eta}}\|}{\bar{m}}, \quad (42)$$

$$\bar{\boldsymbol{\eta}} \equiv \bar{\mathbf{Q}} - \boldsymbol{\beta}, \quad \bar{\mathbf{Q}} \equiv \frac{\bar{\boldsymbol{\sigma}}^*}{\bar{p}}. \quad (43)$$

The inherent or induced anisotropic hardening variable \mathbf{H} is selected as the rotational hardening variable $\boldsymbol{\beta}$. \bar{m} is the stress ratio in the critical state, which is generally a function f_m of

$$\sin 3\bar{\theta}_\sigma \equiv -\sqrt{6} \frac{\text{tr} \bar{\boldsymbol{\eta}}^3}{\|\bar{\boldsymbol{\eta}}\|^3}, \quad (44)$$

including the material constant ϕ_c referred to the frictional angle in the critical state for the axisymmetric compression, i.e.

$$\bar{m} = f_m(\sin 3\bar{\theta}_\sigma; \phi_c). \quad (45)$$

Let the function of the similarity-center surface be described by the following equation in a similar form as Eq. (41) of the subloading surface:

$$f(\hat{\boldsymbol{\sigma}}, \boldsymbol{\beta}) = p_s(1 + \chi_s^2), \quad (46)$$

where

$$\hat{\boldsymbol{\sigma}}^* \equiv \hat{\boldsymbol{\sigma}} + p_s\mathbf{I}, \quad p_s \equiv -\frac{1}{3} \text{tr} \hat{\boldsymbol{\sigma}}, \quad \chi_s \equiv \frac{\|\boldsymbol{\eta}_s\|}{m_s}, \quad (47)$$

$$\boldsymbol{\eta}_s \equiv \mathbf{Q}_s - \boldsymbol{\beta}, \quad \mathbf{Q}_s \equiv \frac{\hat{\boldsymbol{\sigma}}^*}{p_s}. \quad (48)$$

m_s is a function f_m of

$$\sin 3\theta_s \equiv -\sqrt{6} \frac{\text{tr} \boldsymbol{\eta}_s^3}{\|\boldsymbol{\eta}_s\|^3}, \quad (49)$$

including the material constant ϕ_c , i.e.

$$m_s = f_m(\sin 3\theta_s; \phi_c). \quad (50)$$

The evolution rule of rotational hardening variable $\boldsymbol{\beta}$ is given by

$$\dot{\boldsymbol{\beta}} = b_r \|\mathbf{D}^p\| \|\bar{\boldsymbol{\eta}}\| \bar{\boldsymbol{\eta}}_b, \quad (51)$$

where

$$\bar{\eta}_b \equiv \bar{m}_b \bar{t} - \beta, \quad \bar{t} \equiv \frac{\bar{\eta}}{\|\bar{\eta}\|}. \quad (52)$$

\bar{m}_b is also a function f_m of $\bar{\theta}_\sigma$ including the material constant ϕ_b , i.e.

$$\bar{m}_b = f_m(\sin 3\bar{\theta}_\sigma; \phi_b). \quad (53)$$

b_r and ϕ_b are material constants describing the intensity of rotational hardening and the limitation of the rotation of subloading surface, called the *rotational limit angle*, respectively.

The isotropic hardening/softening function F is given by

$$F = F_0 \exp\left(\frac{H}{\rho - \gamma}\right), \quad (54)$$

where F_0 is the initial value of F . ρ and γ are material constants describing the slope of the normal-consolidation and the swelling lines, respectively, in the $(\ln v, \ln p)$ space (v : volume) (Hashiguchi, 1974, 1995). The evolution rule of the isotropic hardening/softening variable H applicable to not only clays but also sands is given by

$$\dot{H} = -D_v^p + \mu \|\mathbf{D}^{p*}\| \left(\frac{\|\boldsymbol{\sigma}^*\|}{p} - m_d \right), \quad (55)$$

where

$$D_v^p \equiv \text{tr } \mathbf{D}^p, \quad (56)$$

$$p \equiv -\frac{1}{3} \text{tr } \boldsymbol{\sigma}. \quad (57)$$

m_d is given as

$$m_d = f_m(\sin 3\theta_\sigma; \phi_d), \quad (58)$$

where

$$\sin 3\theta_\sigma \equiv -\sqrt{6} \frac{\text{tr } \boldsymbol{\sigma}^{*3}}{\|\boldsymbol{\sigma}^*\|^3}. \quad (59)$$

μ and ϕ_d are material constants describing the isotropic hardening/softening behavior induced by the plastic deviatoric deformation. The softening and the hardening are induced by the plastic deviatoric deformation for the state of stress inside and outside, respectively, the surface:

$$\frac{\|\boldsymbol{\sigma}^*\|}{p} = m_d, \quad (60)$$

which is called the *shear boundary surface*.

Let the function ξ in the tangential inelastic modulus T be assumed as

$$\xi = \frac{p}{a\bar{\chi}^c}, \quad (61)$$

where a and c are material constants.

The elastic bulk and shear moduli are given as

$$K = \frac{p}{\gamma}, \quad G = \frac{3(1-2\nu)}{2(1+\nu)} K, \quad (62)$$

where ν is *Poisson's ratio*.

Yield Surface

It is desirable for the shape of the yield surface to fulfill convexity and smoothness in order to answer the principle of maximum plastic work (Hill, 1950) and the linear relation between stress rate and strain rate. In this study, the following equation proposed by Hashiguchi (Hashiguchi, 2002) is adopted as the function \bar{m} fulfilling the aforementioned requirements.

$$\bar{m} = \frac{14\sqrt{6} \sin \phi_c}{(3 - \sin \phi_c)(8 - \sin 3\theta_\sigma)}. \quad (63)$$

The convex-conical surfaces $\|\bar{\mathbf{Q}}\| = \bar{m}$ of Eq. (63) in π -plane for $\phi_c = 15^\circ, 30^\circ, 45^\circ$ are depicted in Fig. 3 comparing with the Mohr-Coulomb failure criterion.

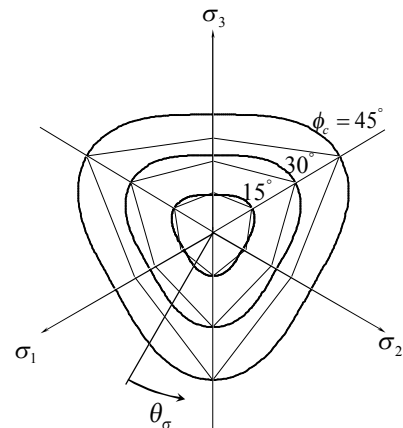


Fig. 3 π -sections of conical surfaces by Hashiguchi

The surfaces fulfill the smooth convexity for any frictional angle ϕ_c as shown in the figure, while it gives rise to a slightly higher frictional angle in the axisymmetric extension state than that in the axisymmetric compression state for a high frictional angle.

Here, Eqs. (50), (53) and (58) are given, respectively, as follows:

$$m_s = \frac{14\sqrt{6} \sin \phi_c}{(3 - \sin \phi_c)(8 - \sin 3\theta_s)}, \quad (64)$$

$$\bar{m}_b = \frac{14\sqrt{6} \sin \phi_b}{(3 - \sin \phi_b)(8 - \sin 3\theta_\sigma)}, \quad (65)$$

$$m_d = \frac{14\sqrt{6} \sin \phi_d}{(3 - \sin \phi_d)(8 - \sin 3\theta_\sigma)}. \quad (66)$$

COMPARISONS WITH EXPERIMENTS

Proportional Loading

The experimental results (Tatsuoka et al. 1986; Paradhan et al. 1989) on Toyoura sand widely used in Japan for the study of the strength and deformation characteristics of sands are used for comparison with calculations. The sand consists mostly of quartz (around 90%) and chert (around 4%) (Yoshimi et al., 1978), and no fines content less than $74\mu\text{m}$ are included. The particles have an angular to sub-angular shape. The physical properties are listed in Table 1. The experimental results for the cyclic loading are the triaxial tests data performed under the drained and undrained conditions. The test procedures and the specimen preparation methods are described by Tatsuoka et al. (1986) and Paradhan et al. (1989), respectively.

The predicted results for the axisymmetrically cyclic loadings under the undrained condition for the dense specimen and the drained condition for the loose specimen are compared in Fig. 4 and 5 respectively with the experimental results. The experimental results in Fig. 4 are indicated for the first and third cycles. The material constants and the initial values for the dense and loose specimens of Toyoura sand are selected as follows:

Table 1 Physical properties of Toyoura sand (Paradhan et al. 1989)

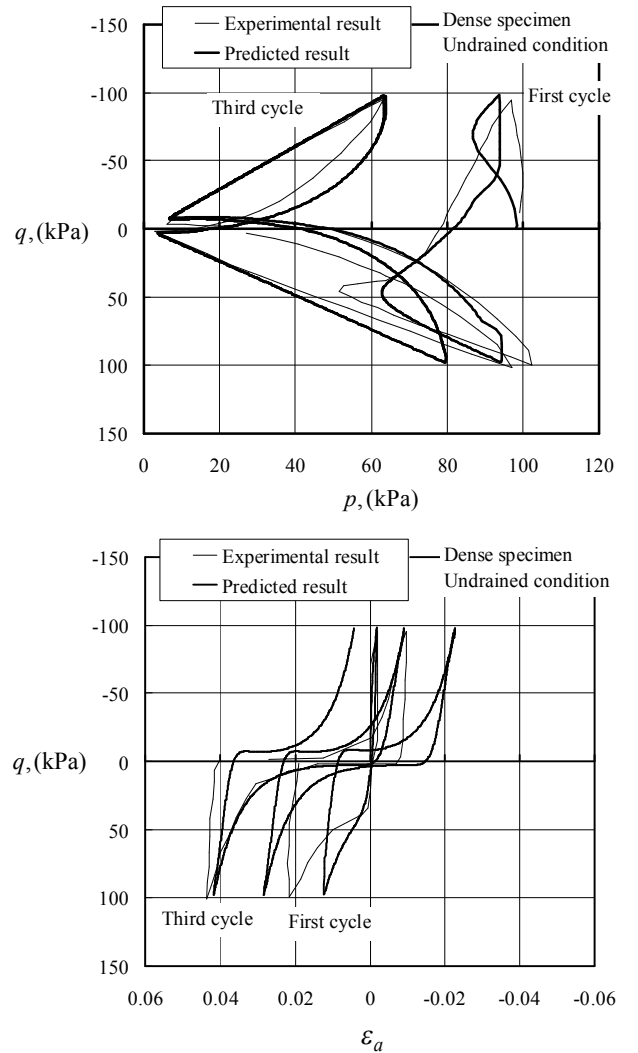
Toyouira sand	
Mean grain size	0.16 mm
Uniformity coefficient	1.46
Specific gravity	2.64
Maximum void ratio	0.977
Minimum void ratio	0.605

Dense specimen

$$\begin{aligned} \phi_c &= 32.0^\circ, \rho = 0.0021, \gamma = 0.0011, u_R = 15, \nu = 0.3, \\ c_s &= 100, \phi_b = 20^\circ, b_r = 100, \phi_d = 28^\circ, \mu = 0.9, \\ \mathbf{s}_0 &= \mathbf{0}, F_0 = 400.0\text{kPa}, \boldsymbol{\sigma}_0 = -29.4\text{IkPa}. \end{aligned}$$

Loose specimen

$$\begin{aligned} \phi_c &= 32.0^\circ, \rho = 0.005, \gamma = 0.0017, u_R = 10, \nu = 0.3, \\ c_s &= 1, \phi_b = 17^\circ, b_r = 80, \phi_d = 30^\circ, \mu = 0.9, \\ \mathbf{s}_0 &= \mathbf{0}, F_0 = 30.0\text{kPa}, \boldsymbol{\sigma}_0 = -29.4\text{IkPa}. \end{aligned}$$



$$q = \sigma_a - \sigma_r, \sigma_a : \text{axial stress}, \sigma_r : \text{radial stress} \\ p : \text{mean principal stress}, \varepsilon_a : \text{axial strain}$$

Fig. 4 The cyclic triaxial test with the constant stress amplitude $q = \pm 98 \text{ kPa}$ under the undrained condition for the dense specimen (Tatsuoka et al. 1986).

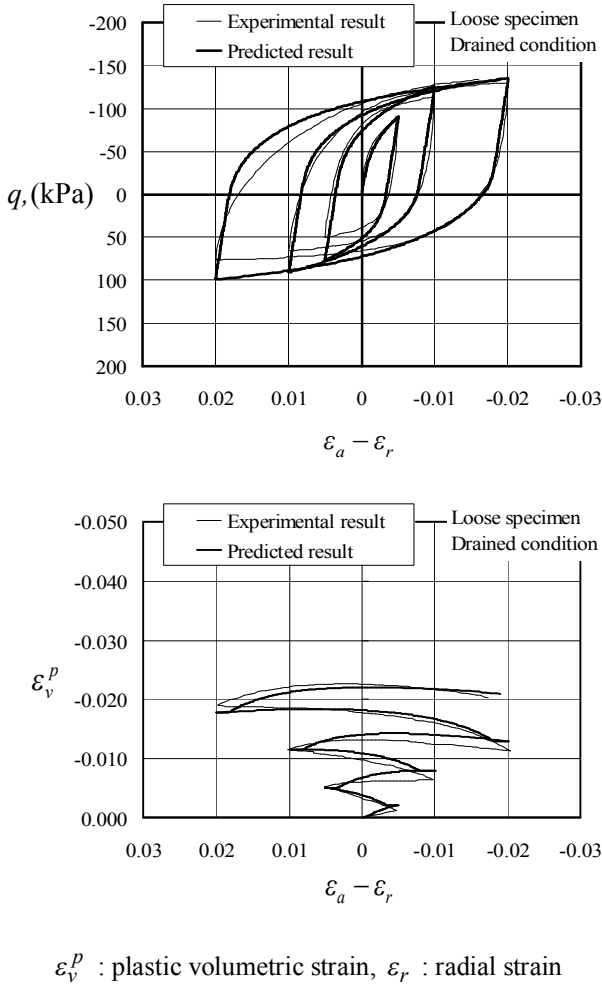


Fig. 5 The cyclic triaxial test performed at a constant $p(=98.1\text{kPa})$ under drained condition for the loose specimen (Paradhan et al. 1989).

The predicted strength and deformation simulate well with the experimental results for both the undrained and drained conditions, and then the hysteresis loops due to the cyclic loadings are realistically described. Thus, the cyclic loading behavior is properly described by the extended subloading surface model which has several pertinent concepts, i.e. an associated flow rule, a subloading surface, rotational hardening, the translation of the similarity-center of the normal-yield and the subloading surfaces.

Nonproportional Loading

The loading of the circular stress path in π -plane in which the deformation of the tangential stress rate direction is remarkably generated is studied in the analysis of the nonproportional loading. The test data under the drained condition by the true triaxial apparatus for Hostun sand and Reid Bedford sand (Saada and Bianchini, 1989) are used

for comparison with calculations. Hostun sand and Reid Bedford sand are a poorly graded material with uniform grain size. The tested specimens were prepared in the dense state with the relative density $Dr=97\%$ for the Hostun sand and in the medium state with the relative density $Dr=47\%$ for Reid Bedford sand under the initial isotropic states of stress $\sigma_0=-100\text{I kPa}$, respectively. The physical properties of these sands are listed in Table 2.

The co-ordinate system (x_1, x_2, x_3) for the true triaxial test apparatus is taken as shown in Fig. 6 where $\sigma_1, \sigma_2, \sigma_3$ are principal stresses.

For the loading of the circular stress path in π -plane, the principal stresses are varied individually leading to the circular stress path in π -plane, keeping the magnitude of the deviatoric stress $\|\sigma^*\|$ and the mean stress σ_m constant as shown in Fig. 7.

Table 2 Physical properties of Hostun sand and Reid Bedford sand.

	Reid Bedford sand	Hostun sand
Grain density	2.65 g/cm ³	2.67 g/cm ³
Maximum density	1.74 g/cm ³	1.66 g/cm ³
Minimum density	1.46 g/cm ³	1.35 g/cm ³
Mean grain size	0.25mm	0.35mm
Uniformity coefficient	1.47	1.68

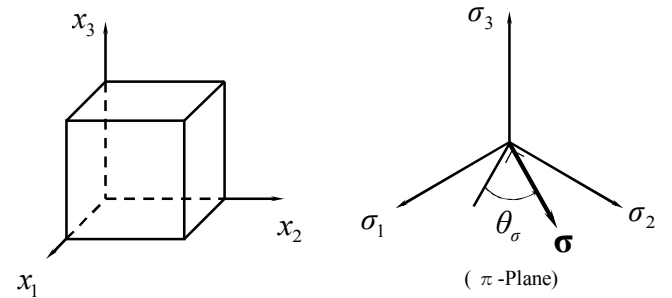


Fig. 6 Rectangular co-ordinates (x_1, x_2, x_3) and the variables for the true triaxial test apparatus

The principal stresses are varied sinusoidally as follows:

$$\sigma_1 = \sigma_m + \sqrt{\frac{2}{3}} \|\sigma^*\| \cos \theta_\sigma, \quad (67)$$

$$\sigma_2 = \sigma_m + \sqrt{\frac{2}{3}} \|\sigma^*\| \cos \left(\theta_\sigma - \frac{2}{3} \pi \right), \quad (68)$$

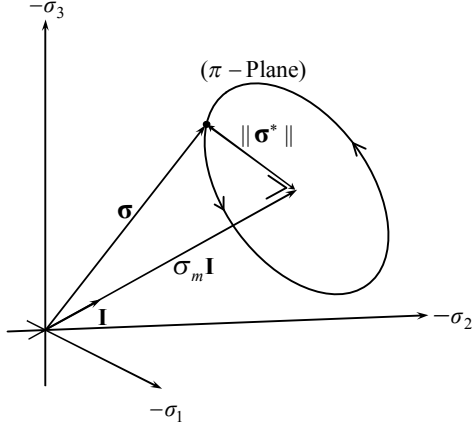


Fig. 7 Circular stress path in deviatoric stress plane

$$\sigma_3 = \sigma_m + \sqrt{\frac{2}{3}} \|\boldsymbol{\sigma}^*\| \cos\left(\theta_\sigma + \frac{2}{3}\pi\right). \quad (69)$$

The stress changes are given by

$$\Delta\sigma_1 = -\sqrt{\frac{2}{3}} \|\boldsymbol{\sigma}^*\| \sin\theta_\sigma \Delta\theta_\sigma, \quad (70)$$

$$\Delta\sigma_2 = -\sqrt{\frac{2}{3}} \|\boldsymbol{\sigma}^*\| \sin\left(\theta_\sigma - \frac{2}{3}\pi\right) \Delta\theta_\sigma, \quad (71)$$

$$\Delta\sigma_3 = -\sqrt{\frac{2}{3}} \|\boldsymbol{\sigma}^*\| \sin\left(\theta_\sigma + \frac{2}{3}\pi\right) \Delta\theta_\sigma. \quad (72)$$

$\|\boldsymbol{\sigma}^*\|$ and σ_m are 420kPa and -500kPa for Hostun sand and 262kPa and -345kPa for Reid Bedford sand, respectively. The stress phase angle θ_σ is varied from 30 to 750 degree realizing the two cycles for both Hostun and

Reid Bedford sands

The material constants and the initial values for Hostun sand and Reid Bedford sand are respectively selected as follows:

Hostun sand

$$\begin{aligned} \phi_c &= 30.0^\circ, \rho = 0.008, \gamma = 0.0035, u_R = 60, \nu = 0.3, \\ c_s &= 50, \phi_b = 24^\circ, b_r = 40, \phi_d = 31^\circ, \mu = 1, \\ \mathbf{s}_0 &= 20\mathbf{I}\text{kPa}, F_0 = 600.0\text{kPa}, \boldsymbol{\sigma}_0 = -100.0\mathbf{I}\text{kPa} \\ a &= 0.018, b = 5, c = 1. \end{aligned}$$

Reid Bedford sand

$$\begin{aligned} \phi_c &= 27.0^\circ, \rho = 0.0055, \gamma = 0.0018, u_R = 34, \nu = 0.3, \\ c_s &= 19, \phi_b = 20^\circ, b_r = 70, \phi_d = 27^\circ, \mu = 0.8, \\ \mathbf{s}_0 &= \mathbf{0}, F_0 = 425.0\text{kPa}, \boldsymbol{\sigma}_0 = -100.0\mathbf{I}\text{kPa} \\ a &= 0.009, b = 1, c = 1. \end{aligned}$$

The strain paths in π -plane predicted from the elastic strain rate and the plastic strain rate by the extended subloading surface model without the tangential strain rate for Hostun sand and Reid Bedford sand are respectively compared in Fig. 8 with the experimental results. It is observed in both the experimental results and the predicted results that the strain paths with the shape of two triangles by two cyclic loadings are depicted. The triangles for the experimental strain paths relatively incline in the counter-clockwise direction with those for the predicted results, and the predicted deformation behavior are undoubtedly different from the experimental results. The stiffness of stress rate direction in the counter-clockwise is specifically predicted high.

The direction and magnitude of the inelastic strain rate

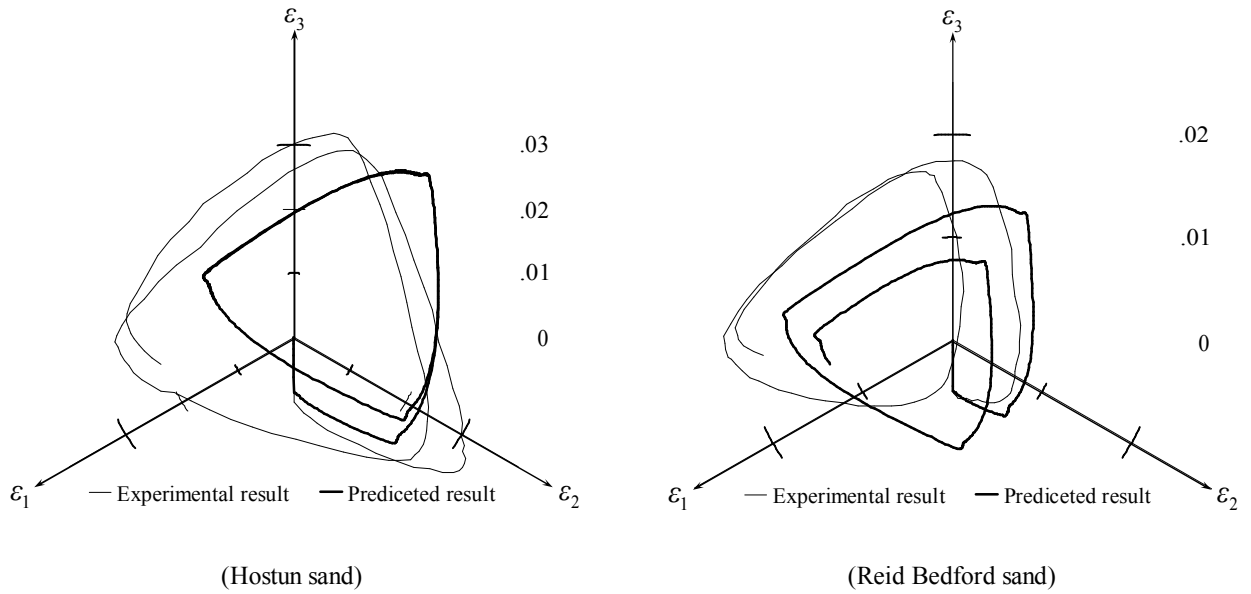


Fig. 8 Strain paths in the π -plane by the extended subloading surface model without the tangential strain rate

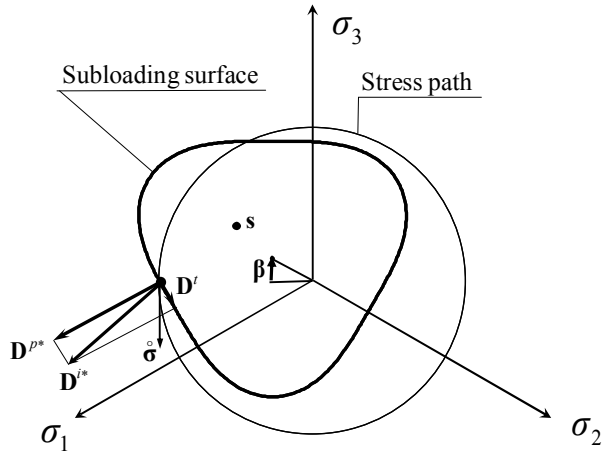


Fig. 9 The inelastic strain rate \mathbf{D}^i in π -plane at $\theta_{\sigma}=300^{\circ}$ for Hostun sand.

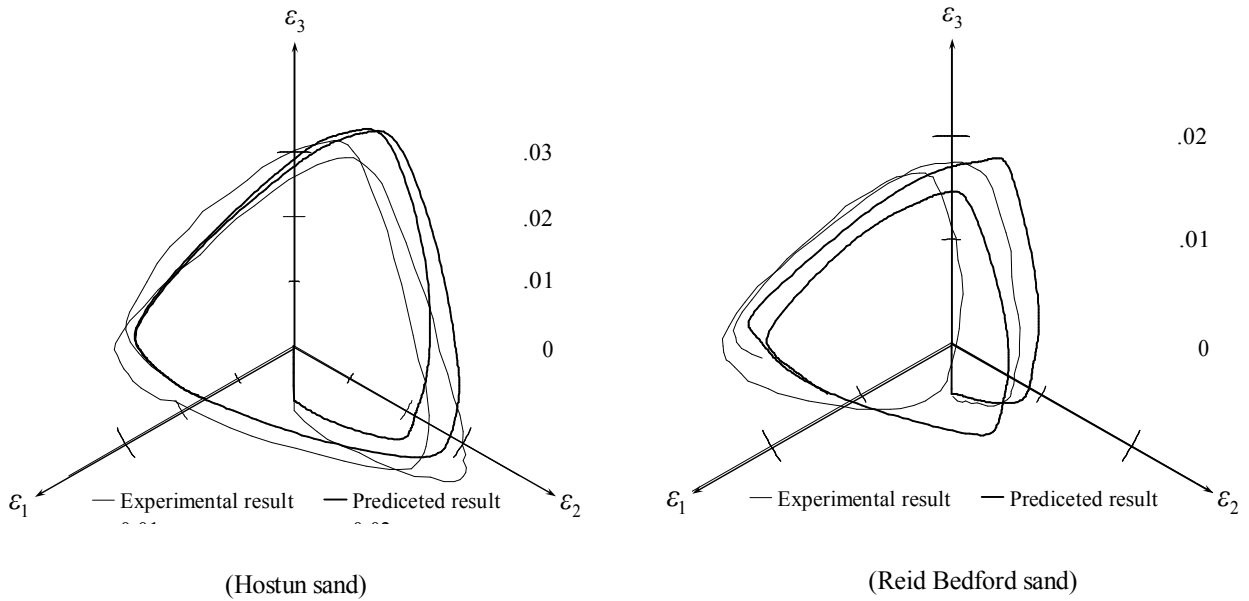


Fig. 10 Strain paths in the π -plane by the extended subloading surface model with the tangential strain

\mathbf{D}^i at the stress phase angle $\theta_{\sigma} = 300^{\circ}$ predicted by the extended subloading surface model with the tangential strain rate for Hostun sand is represented as the vector in Fig. 9. The stress path and vectors on the plastic and tangential strain rates \mathbf{D}^p , \mathbf{D}^t are also represented in the figure. The direction of the inelastic strain rate \mathbf{D}^i is induced toward the direction of the stress rate $\dot{\boldsymbol{\sigma}}$ from the direction perpendicular to the subloading surface by the tangential strain rate effect as shown in Fig. 9. The strain paths in π -plane for Hostun sand and Reid Bedford sand predicted by the extended subloading surface model with the tangential strain rate are shown in Fig. 10. It is observed that the stiffness of the stress rate direction is relaxed, and

the strain paths of the experimental results for both Hostun sand and Reid Bedford sand are realistically predicted. The deformation behavior in the first and second cycles is also properly described.

The variations of the predicted principal strains $\varepsilon_1, \varepsilon_2, \varepsilon_3$ for Hostun sand and Reid Bedford sand against the stress phase angle θ_{σ} are compared in Fig. 11 with the experimental results. The variations of principal strains are well simulated for both Hostun sand and Reid Bedford sand, respectively.

On the other hand, the strain paths in the π -plane calculated by the plastic strain rate and the tangential strain rate for Hostun sand are respectively shown in Fig. 12. The

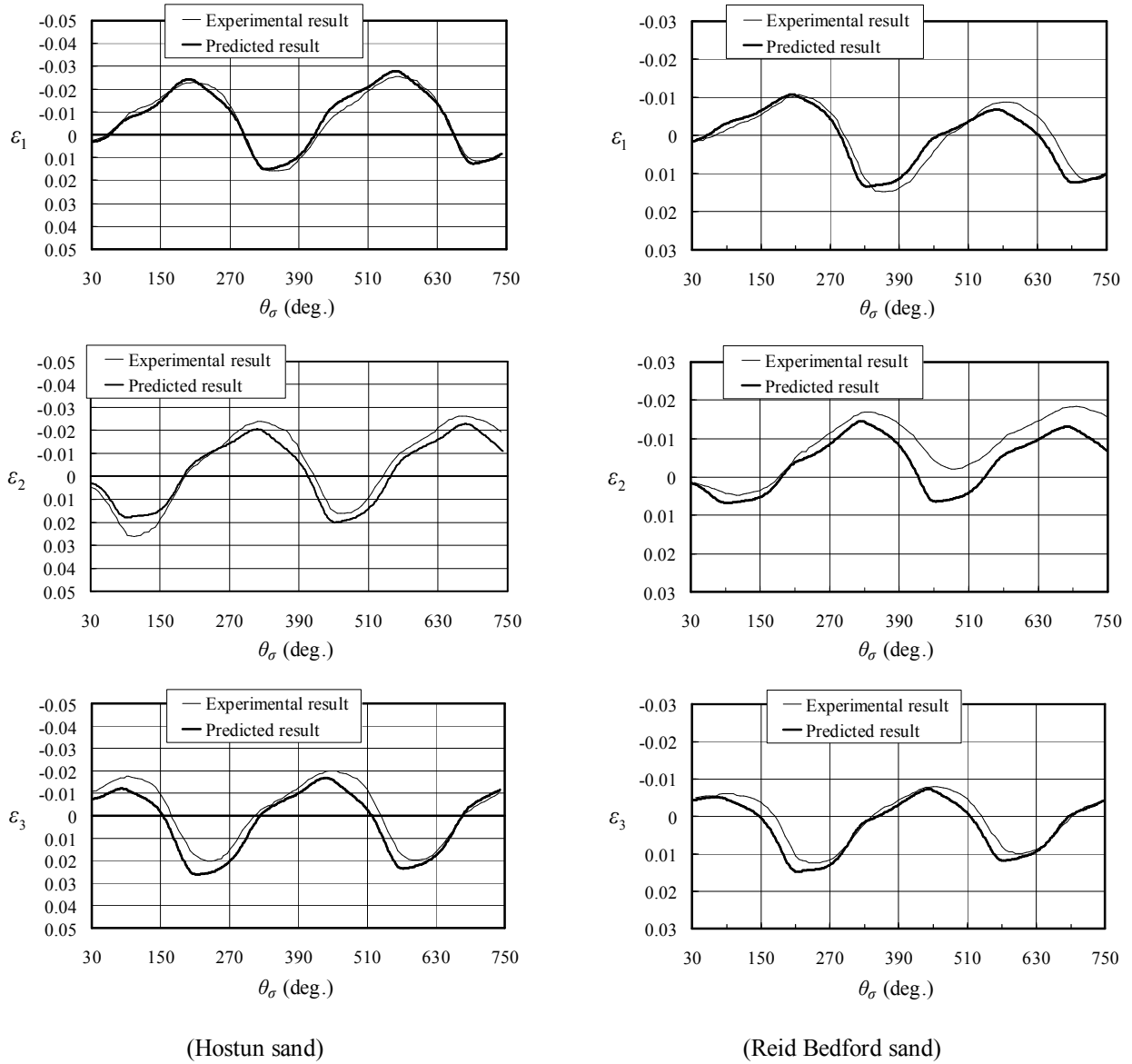


Fig. 11 Variation of three principal strain $\varepsilon_1, \varepsilon_2, \varepsilon_3$ against stress phase angle θ_σ .

strain path due to the plastic strain rate exhibits the shape as if the subloading surface in the π -plane is rotated $\pi/2$ in the clockwise rotation because the plastic strain rate occurs perpendicular to the subloading surface according to the associated flow rule. The tangential strain rate is induced by the deviatoric stress rate tangential to the subloading surface, and the strain path exhibits the similar shape of the subloading surface in the π -plane. For nonproportional loading, it is required to adopt the equation of yield surface with the appropriate shape, since the stress translates along the yield surface and the predicted inelastic strain rate is directly dependent on the shape of the yield surface. Especially, for the nonproportional loading in the π -plane such as in the present study, the equation of yield surface with appropriate cross-sectional shape in the π -plane should be incorporated into the constitutive equation.

CONCLUSIONS

The extended subloading surface model with the tangential strain rate was applied to the cyclic loading behavior in the nonproportional loading for sands. The cyclic loading behavior in the proportional loading are realistically predicted by the extended subloading surface model which has several pertinent concepts, i.e. an associated flow rule, a subloading surface, rotational hardening, the translation of the similarity-center. On the other hand, for the cyclic loading under the nonproportional loading of the circular stress path in π -plane, the extended subloading surface model which is independent of the magnitude and direction of the stress rate in the inelastic strain rate predicts the stiffness of the direction of stress rate high. The subloading surface model with the tangential

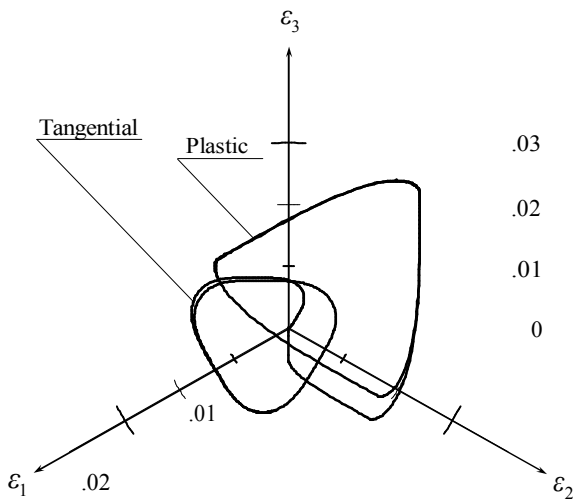


Fig. 12 Plastic and tangential strain paths in π -plane for Hostun sand

strain rate properly describes the deformation of the stress rate direction and then predicts realistically the experimental deformation behavior. The extended subloading surface model with the tangential strain rate is applicable to the realistic prediction of the cyclic loading behavior for the nonproportional loading. Besides, it is indicated that the yield surface with the appropriate shape should be incorporated into the constitutive equation for the analysis of the nonproportional loading since the stress translates along the yield surface.

REFERENCES

- Dafalias, Y. F. (1985). The plastic spin, *J. Appl. Mech. (ASME)*, 52, 865-871.
- Drucker, D. C. (1988). Conventional and unconventional plastic response and representation, *Appl. Mech. Rev. (ASME)*, 41, 151-167.
- Hashiguchi, K. (1974). Isotropic hardening theory of granular media, *Proc. JSCE*, No.227, 45-60.
- Hashiguchi, K. and Ueno, M. (1977). Elastoplastic constitutive laws of granular materials, *Constitutive Equations of Soils (Proc. 9th Int. conf. Soil Mech. Found. Eng., Spec. Session 9, Tokyo)*, JSSMFE, 73-82.
- Hashiguchi, K. (1980). Constitutive equations of elastoplastic materials with elastic-plastic transition, *J. Appl. Mech. (ASME)*, 47, 266-272.
- Hashiguchi, K. (1989). Subloading surface model in unconventional plasticity, *Int. J. Solids Struct.*, 25, 917-945.
- Hashiguchi, K. (1993a). Fundamental requirements and formulation of elastoplastic constitutive equations with tangential plasticity, *Int. J. Plasticity*, 9, 525-549.
- Hashiguchi, K. (1993b). Mechanical requirements and structures of cyclic plasticity models, *Int. J. Plasticity*, 9, 721-748.
- Hashiguchi, K. (1995). On the linear relation of $V\text{-ln}p$ and $\ln v\text{-ln}p$ for isotropic consolidation of soils, *Int. J. Numer. Anal. Meth. Geomech.*, 19, 367-376.
- Hashiguchi, K. and Yoshimaru. (1995). A generalized formulation of the concept of nonhardening region, *Int. J. Plasticity*, 11, 347-365.
- Hashiguchi, K. and Chen, Z.-P. (1998). Elastoplastic constitutive equations of soils with the subloading surface and the rotational hardening, *Int. J. Numer. Anal. Meth. Geomech.*, 22, 197-227.
- Hashiguchi, K. (2000). Fundamentals in constitutive equation: continuity and smoothness conditions and loading criterion, *Soils and Foundations*, 40(4), 155-161.
- Hashiguchi, K. and Tsutsumi, S. (2001). Elastoplastic constitutive equation with tangential stress rate effect, *Int. J. Plasticity*, 17, 117-145.
- Hashiguchi, K. (2001). Description of inherent/induced anisotropy of soils: Rotational hardening rule with objectivity, *Soils and Foundations*, 41 (6), 139-145.
- Hashiguchi, K. (2002). A Proposal of the simplest convex-conical surface for soils, *Soils and Foundations*, 42(3), 107-113.
- Hashiguchi, K. and Tsutsumi, S. (2003). Shear band formation analysis in soils by the subloading surface model with tangential stress rate effect, *Int. J. Plasticity*, 19, 1651-1677.
- Hashiguchi, K. and Protasov, A. (2004). Localized necking analysis by the subloading surface model with tangential-strain rate and anisotropy, *Int. J. Plasticity*, 20, 1909-1930.
- Hill, R. (1950). *The Mathematical Theory of Plasticity*, Clarendon Press.
- Khojastehpour, M. and Hashiguchi, K. (2004a). Axisymmetric bifurcation analysis in soils by the tangential-subloading surface model, *J. Mech. Physics of Solids*, In Press.
- Khojastehpour, M. and Hashiguchi, K. (2004b). Plane strain bifurcation analysis of soils by the tangential-subloading surface model, *Int. J. Solids Struct.*, 41, 5541-5563.
- Masing, G. (1926). Eigenspannungen und Verfestigung beim Messing, *Int. Proc. 2nd Int. Congr. Appl. Mech.*, Zurich, 332-335.
- Mroz, Z. (1966). On forms of constitutive laws for elastic-plastic solids, *Archiwum Mechaniki Stosowanej*, 18, 1-34.
- Paradhan, T. B. S., Tatsuoka, F. and Sato, Y. (1989). Experimental stress-dilatancy relations of sand subjected to cyclic loading, *Soils and Foundations*, 29 (1), 45-64.

- Rudnicki, J. W. and Rice, J. R. (1975). Conditions for localization of deformation in pressure-sensitive dilatant materials, *J. Mech. Phys. Solids*, 23, 371-394.
- Saada, A. S. and Bianchini, G. (1989). *Proc. Int. Workshop on Constitutive Equations for Granular Non-cohesive Soils*, Cleveland, Balkema, Rotterdam.
- Tatsuoka, F., Toki, S., Miura, S., Kato, H., Okamoto, M., Yamada, S., Yasuda, S. and Tanizawa, F. (1986). Some factors affecting cyclic undrained triaxial strength of sand, *Soils and Foundations*, 26 (3), 99-116.
- Topolnicki, M. (1990). An elasto-plastic subloading surface model for clay with isotropic and kinematic mixed hardening parameters, *Soils and Foundations*, 30, pp. 103-113.
- Yoshimi, Y., Hatanaka, M. and Oh-Oka, H. (1978). Undisturbed sampling of saturated sand by freezing, *Soils and Foundations*, 18 (3), 59-73.
- Zbib, H. M. and Aifantis, E. C. (1988). On the concept of relative and plastic and its implications to large deformation theories. Part I: Hypoelasticity and vertex-type plasticity *Acta. Mech.*, 75, 15-33.

